Experimental Investigation of Two Conventional Energy Harvesting Eels in Tandem Configuration

Author

Ahmad Mujtaba Khan

Registration Number

00000171809

Supervisor

Dr. Emad Uddin

DEPARTMENT OF MECHANICAL ENGINEERING

SCHOOL OF MECHANICAL & MANUFACTURING ENGINEERING

NATIONAL UNIVERSITY OF SCIENCES AND TECHNOLOGY

ISLAMABAD

DECEMBER, 2019

Experimental Investigation of Two Conventional Energy Harvesting Eels in Tandem Configuration

Author

Ahmad Mujtaba Khan

Registration Number

00000171809

A thesis submitted in partial fulfillment of the requirements for the degree of

MS Mechanical Engineering

Thesis Supervisor:

Dr. Emad Uddin

Thesis Supervisor's Signature: _____

DEPARTMENT OF MECHANICAL ENGINEERING

SCHOOL OF MECHANICAL & MANUFACTURING ENGINEERING

NATIONAL UNIVERSITY OF SCIENCES AND TECHNOLOGY,

ISLAMABAD

DECEMBER, 2019

THESIS ACCEPTANCE CERTIFICATE

Certified that final copy of MS thesis written by Mr./Mrs. _____ (Registration No. _____), of _____ (School/College/Institute) has been vetted by undersigned, found complete in all respects as per NUST Statutes / Regulations, is free of plagiarism, errors, and mistakes and is accepted as partial fulfillment for award of MS/MPhil degree. It is further certified that necessary amendments as pointed out by GEC members of the scholar have also been incorporated in the said thesis.

Signature: _____

Name of Supervisor: _____

Date:_____

Signature (HOD): _____

Date:_____

Signature (Dean/Principal): _____

Date:_____

FORM TH-4

MASTER THESIS WORK

We hereby recommend that the dissertation prepared under our supervision by: (Student Name & Regn No.)_____

Titled: _____be accepted in partial fulfillment of the requirements for the award of _____degree.

Examination Committee Members

1. Name:_____ Signature:_____

2. Name:_____ Signature:_____

3. Name:_____ Signature:_____

Supervisor's name: _____ Signature:_____
Date:_____

_____ _____
Head of Department Date

COUNTERSINGED

_____ _____
Date Dean/Principal

Plagiarism Certificate (Turnitin Report)

This thesis has been checked for Plagiarism. Turnitin report endorsed by Supervisor is attached.

Signature of Student

ABC

Registration Number

Signature of Supervisor

DECLARATION

I certify that this research work titled "*Energy Harvesting of Two Conventional Piezoelectric Flags in Tandem Configuration"* is my own work. The work has not been presented elsewhere for assessment. The material that has been used from other sources it has been properly acknowledged/referred.

Signature of Student
Ahmad Mujtaba Khan
00000171809

LANGUAGE CORRECTNESS CERTIFICATE

This thesis has been read by an English expert and is free of typing, syntax, semantic, grammatical and spelling mistakes. The thesis is also according to the format given by the university.

Signature of Student
Ahmad Mujtaba Khan
00000171809

COPYRIGHT STATEMENT

ACKNOWLEDGMENT

I am thankful to my Creator Allah Subhana-Watala to have guided me throughout this work at every step and for every new thought which You set up in my mind to improve it. Indeed I could have done nothing without Your priceless help and guidance. Whosoever helped me throughout the course of my thesis, whether my parents or any other individual was Your will, so indeed none be worthy of praise but You.

I am profusely thankful to my beloved parents who raised me when I was not capable of walking and continued to support me throughout every department of my life.

I would also like to express special thanks to my supervisor Dr. Emad Uddin for his help throughout my thesis and also for the Advance Fluid Mechanics course which he has taught me.

I would also like to pay special thanks to Usman Latif, Ehtisham Ali, Muhammad Umair and Hammas Ullah for their help and support. Each time I got stuck in something, they proposed the best solution. I appreciate their patience and guidance throughout the whole thesis.

I am thankful to Dr. Muhammad Sajid, Dr. Samiur Rahman Shah, and Dr. Zaib Ali, for being on my thesis guidance and evaluation committee.

Finally, I would like to express my gratitude to all the individuals who have rendered valuable assistance to my study.

Dedicated to my loving parents, adored siblings, and friends whose tremendous support and cooperation led me to this wonderful accomplishment.

ABSTRACT

The interaction of two tandem conventional piezoelectric flag configuration in a uniform flow was investigated. The piezoelectric flags convert the kinetic energy of flowing water into electrical energy based on vortex-induced vibration. The piezoelectric flags were placed in the wake of a bluff body and their flapping behavior is investigated in terms of the flow velocity and streamwise gap between flags. The flags showed two types of flapping modes; flapping mode and biased mode. Inverted drafting was observed in flags: the drag force on one flag is increased by excitation from the wake of others. The output voltage of flags increased by increasing the flow velocity because the forces applied on the piezoelectric flag increases by increasing the flow velocity. The flapping amplitude and output voltage of the downstream flag is found to be larger than the upstream flag. The experiments were performed by placing two conventional piezoelectric flags in tandem configuration in the wake of bluff body in low-speed water tunnel by varying the flow velocity (V) and streamwise gap (G_x) behind an inverted C shaped cylinder to find the effect of vortices produced from the bluff body on flapping amplitude, flapping frequency and the voltage generated by the piezoelectric flags. Image processing technique was used to find out peak to peak amplitude and Fast Fourier Transform (FFT) was used to find out a dominant flapping frequency in MATLAB. The output voltage from the piezoelectric flag was measured by using DAQ (a module in Lab View for receiving analog output voltage).

TABLE OF CONTENTS

LIST OF FIGURES

List of Tables

CHAPTER 1: INTRODUCTION

Renewable energy sources have drawn a lot of attention nowadays because of the effect of increasing global warming and the increasing demand for fossils fuels. The structures which are subjected to fluid flow are usually designed to minimize fatigue caused by vortex-induced vibrations. Nowadays it is desirable to enhance the vibrations in order to acquire maximum energy from the fluid flow. If we place a bluff body in a flowing fluid then the flow over this bluff body generates alternating vortices. Energy can be harvested from the vortices produced behind a bluff body in a fluid flow because vortex-induced vibrations can extract energy from the fluid flow. Bluff bodies of different shapes, such as circular cylinder, C shaped cylinder, D shaped cylinder or square rod can be used for the generation of vortices. The vortices are generated by placing a bluff body in a unidirectional flow. When a bluff body encounters uniform fluid flow, the flow separates from the surface of the body and wake is formed behind the bluff body. This wake is recognized by two vortices on each side of the body which are shed periodically. This periodic vortex shedding generates unequal pressure distribution around the body. The vortices give an ideal force for the flapping of a piezoelectric flag when placed behind the bluff body. In recent times most of the research has been done on the flapping dynamics of the piezoelectric membranes in a fluid flow. The piezoelectric membrane vibrates when the vortices strike on its surface. The energy conversion is completed in two steps. First, the kinetic energy of the water is converted into the mechanical strain energy of the piezoelectric flag and then strain energy stored in the flag is converted into electrical energy.

1.1 Background, Scope and Motivation

In fluid-structure interaction (FSI) phenomena, the moving fluid interacts with the flexible structures, when fluid comes in contact with the structures. Energy can be harvested from the vortices produced behind a bluff body because they have the potential to extract energy from the flowing fluid. Different kinds of ceramic-based piezoelectric materials are used for energy harvestings, such as the polyvinylidene fluoride (PVDF) membranes, the active fiber composites, and the macro fiber composites [11]. Polyvinylidene fluoride (PVDF) membranes are widely used because they show high resistance to fatigue loadings and are more stable.

The process of energy conversion from flowing fluid is completed in two steps. First, the kinetic energy of the flowing fluid is converted into the mechanical strain energy of the flag and then this strain energy stored in the flag is converted into electrical energy through piezoelectric patches attached on the surface of the flag [8]. The flexible flag can be arranged in two different ways in a flowing fluid, a conventional flag configuration in which the leading edge of the flag is clamped and trailing edge is free to move and an inverted flag configuration in which the leading edge of the flag is free to move and trailing edge is clamped. The flapping behavior and dynamics of the conventional flag are completely different from an inverted flag and the flapping amplitude of the inverted flag is larger as compared to a conventional flag at the same flow velocity. The stability of the conventional flag is greater than the inverted flag [5].

There are two types of hydrodynamic behavior shown by piezoelectric flags when they are placed in a fluid flow, where the drag force on one flag is increased or decreased by excitation from the wake of another flag.

Conventional Drafting:

Conventional Drafting is shown by rigid bodies and the drag force on the upstream flag decreases.

Inverted drafting:

Inverted drafting is found in flexible bodies and the drag on the downstream flag increases.

CHAPTER 2: LITERATURE REVIEW

Naturally, the flapping wing of birds flying in the air and motion of fish with fins swimming in the water behave like a flexible structure in flowing fluid and their motion affects the motion of other birds and fish behind it because they interact with the vortices produced from them while swimming and flying.

The flexible piezoelectric flag can be arranged in two different ways, a conventional flag configuration in which the leading edge of the flag is clamped and trailing edge is free to move and an inverted flag configuration in which the leading edge is free to move and trailing edge of the flag is clamped. The flapping behavior of the conventional flag is completely different from an inverted flag and an inverted flag shows a large flapping amplitude as compared to a conventional flag at the same flow speed. The inverted flag is more unstable than the conventional flag [5].

Many researchers used different configurations with the conventional and inverted flags to improve energy harvesting performance of the piezoelectric flags. They placed the flags in tandem, side by side and multiple flags in diamond or X-shaped configuration for improving the efficiency of energy harvesting from the piezoelectric flags. The flapping amplitude of the downstream flag was found to be larger when both the flag flap at the same flow velocity and at the same time. In the tandem configuration of the flags, the flag placed upstream, strongly influences a downstream flag through vortex shedding in the fluid medium and drag on downstream flag reduces due to the presence of the upstream flag. The difference between the drag force acting on the upstream and downstream flags is explained by the structure of the vortices in the wake of multiple flags. The interaction of the vortices of conventional upstream flag with the downstream flexible flag in the tandem configuration was studied including the bending coefficient, frequency and flapping amplitude of pitching and heaving motion. It was found that the drag coefficient of the downstream flag slightly depends on the gap distance between the two flags [12].

The interaction of the vortices between a conventional flexible flag in uniform flow in triangular, diamond and conical configuration was examined as a function of the bending

coefficient and the gap distance between the flag [19]. Coupling performance of two similar flags in side-by-side, parallel, tandem and staggered position was studied in detail. Significant reductions in drag force were observed for relatively small separation distance between the flags in a parallel position [20].

It was shown by Ristroph & Zhang that in the tandem configuration of flexible flags, the upstream flag experiences a lesser drag force as compared to the downstream flag [10]. Alben then described this anomalous hydrodynamic drafting in his numerical simulation using an inviscid vortex sheet model. He proposed that the wake region behind an upstream flag influences flapping amplitude, and the hydrodynamics drafting was found to be a function of the streamwise gap distance between the piezoelectric flags [13]. He also examined that the vortices shed by the upstream flag placed in the flow interact with the vortices of the downstream flag by two modes of interaction of vortices, which describes the significant changes in drag force experienced by the flexible structures: (i) a constructive mode or (ii) a destructive mode. The drag on the downstream flag depends on the flow velocity and the streamwise gap between the flags. Vortices generated by an upstream rectangular plate induce periodic deformation in the flexible structure, which leads to a lock-in process, synchronization of vortex shedding frequency and the oscillation frequency of the structure [2].

Akaydin investigated the performance of a flexible cantilevered beam as an energy harvester behind an upstream bluff body. He observed the that the energy harvesting performance of the beam was affected by the ratio of vortex shedding frequency to flapping frequency of the beam and the distance between the beam structure and the upstream cylinder [1].

When a bluff body encounters a uniform fluid flow, the flow separates from the boundary surface of the bluff body and generate vortices from both sides and a broad wake. A vortex is a rotating area in a fluid medium that can be defined by many concentric circular layers that rotate with different angular velocity [7]. This wake has two vortices a clockwise and an anticlockwise vortex, which are shed periodically. This periodic vortex shedding produces unequal pressure distribution around the bluff body [6]. Motion is induced in the flexible structures placed behind the bluff body due to the energy of the vortices and change in pressure distribution. As the vortex generation repeats periodically in the fluid flow, therefore, the flexible structure placed behind the bluff body moves continuously due to the continuous vortex shedding.

2.1 Fundamentals of Vortex-Induced Vibrations

Vortex shedding is a widely occurring phenomenon applicable to any bluff body submerged in a fluid flow. Since any real fluid has some viscosity, so there will be a significant boundary layer on the surface of bluff body for the flow at low speeds. At some point along the body, the boundary layer will separate from the surface of the body, depending on the exact surface geometry. This separated layer, which bounds the wake and free stream, will tend to cause fluid to rotate. This rotation then leads to the formation of individual vortices, which are shed from the rear side of the body and travel down the wake. Generally, a pattern of periodic, alternating vortex shedding will occur in the flow behind the body, which is called a vortex street.

2.1.1 Vortex Shedding at Different Reynolds Numbers

Vortex are not generated at low speeds and at low Reynolds Number equal to or less than 5. In 1978 Nishioka experimentally studied the behavior of wake region behind a cylinder at Reynolds Number between 10 and 150. For this purpose, he used a low-speed wind tunnel. He observe that the vortices are generated in this range and the length of vortices increases by increasing the Reynold Number. At Reynolds Number 45, the length of vortices reaches three times the diameter of the cylinder [14].

In 1990 Huerre and Monkewitz investigated the effect of increasing Reynolds Number on the vortices and they proposed that the stability of the wake was disturbed [15]. In 1980 Friehe performed an experiment to study the vortex shedding frequency and velocity of the free stream of fluid flowing over the cylinder, having a length to diameter ratio of greater than 150. The range of Reynolds Number was kept between 50 to 175. It was concluded that vortices start to break in this range [16].

In 1954 Anatol Roshko examined the dynamics of the wake behind circular cylinders in wind tunnel having diameter from 0.0235 to 0.635 cm. The range of Reynold Number was kept

between 40 to 10000. He set two ranges based on the dynamics of the flow. The flow was in the stable range below the Reynolds Number of 150, and viscous forces were dominant and flow was laminar. Beyond the Reynolds Number of 150, the flow was in transition range and flow was turbulent. The boundary was still in the laminar range and only the vortices in the wake region are in turbulent range. Roshko in 1961 noticed an increase in the drag coefficient of a large cylinder placed in a wind tunnel. The vortex shedding started to occur again with the complete turbulence of vortices as well as the boundary layer.

2.1.2 Vortex Shedding across a cylinder

Griffin and Ramberg in 1975 investigated the formation of the wake behind a rigid cylinder. Their studies showed that when the cylinder vibrates with a frequency approximately equals to the vortex shedding frequency, then the vortices are shed with greater strength due to resonance. Bishop and Hassan in 1964 concluded the findings of their experiment and showed that the cylinder experiences more drag force [21].

2.1.3 Vortex Shedding across Flat Plate

Teimourian in 2017 reviewed numerically the vortex shedding behind a flat plate having different arrangements consisting of a single plate, tandem, and side by side configurations. Most of the literature has been studied on a single plate. Among the different turbulent models, direct numerical simulation (DNS) is mostly used by the researchers. Bently and Mudd investigated the effect of vortex shedding and the effect of gap distance for different bluff bodies. They concluded that the bluff bodies that are closely spaced in tandem configuration show the same behavior as a single body. The vortices start to separate from the bluff body and their effect appears as the gap is increased.

2.2 Vortex Generation and Shedding

2.2.1 Vortex Generation

When a bluff body is submerged in a fluid flow at low Reynolds Number i.e. Re $\leq$ 5, the fluid follows the shape of the object all around the body and flows smoothly over the surface of the body. There is an asymmetric configuration of the streamlines around the body with oscillating high pressure at the front and back and low pressure at the top and bottom of the object placed in the fluid flow. When the Reynolds Number becomes greater than 5, the fluid separation starts to occur from the body surface and the vortex generation starts at the back of the body and wake is formed behind the cylinder. The wake is a disturbed fluid medium and has two vortices on each side of the bluff body which are shed periodically.

2.2.2 Vortex Shedding

When the Reynolds Number reaches 100, the vortices start to separate from the surface of the body. These vortices are shed periodically from the bluff body. In the case of multiple flags in tandem or staggered configuration, the vortices shed from the upstream flag interact with the vortices of downstream flag either by constructive or destructive vortex merging mode, depending on the gap between the flags and velocity of the flow. The flapping amplitude and the drag force of the downstream flag increases or decreases, which depends upon the merging mode of the vortices. Lienhard in 1966 studied the vortex generation and vortex shedding behind the cylinder at different Reynolds Number as shown in figure [17].

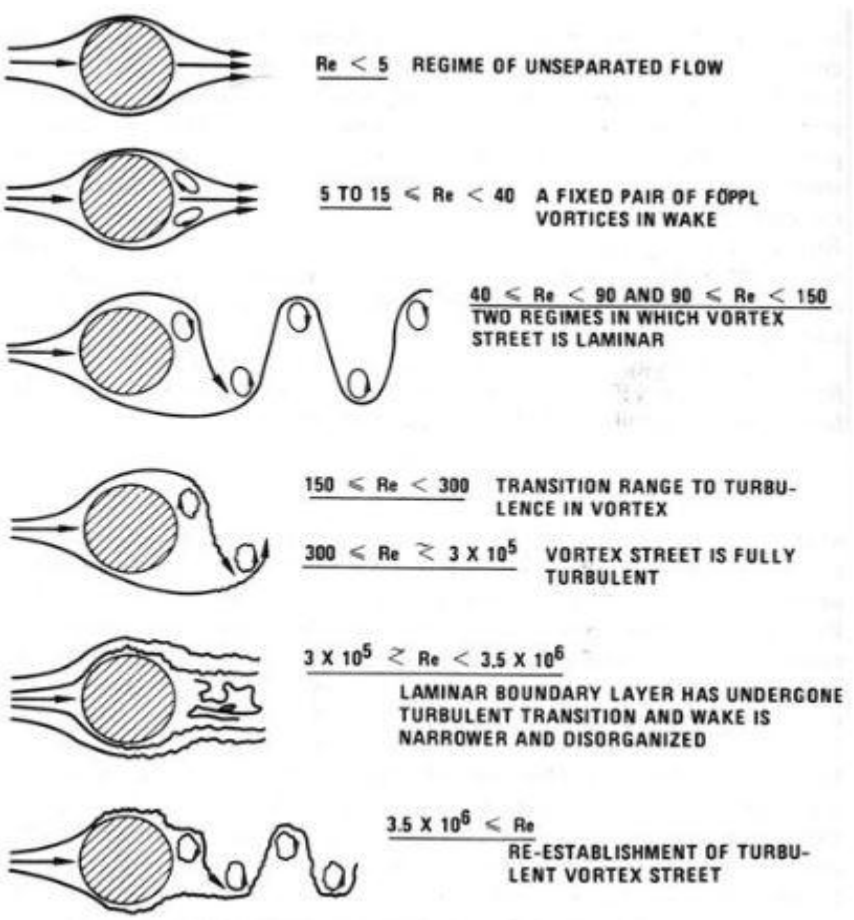

Figure 2.1: Vortex shedding at different Reynolds Number behind a circular cylinder.

2.3 Blockage Ratio

Choi in 1998 experimentally investigated the blockage ratio of a square model wind tunnel. The blockage ratio is defined as the ratio of the diameter of the cylinder used to the width of the tunnel. If the blockage ratio increases, the thickness of the boundary layer increases. He concluded in his research that the blockage ratio can be allowed up to 10% which has negligible effects on the experiments performed [18].

2.4 Basic Definitions

2.4.1 Viscosity

It is also known as absolute viscosity or dynamic viscosity. It is the property of a fluid that offers resistance to the movement between the adjacent layers of fluid. Its unit is N-s/m^2.

2.4.2 Kinematic Viscosity

It is the ratio of dynamic viscosity of fluid to the density of the fluid. The unit of kinematic viscosity is m^2/s.

2.4.3 Angle of Attack

It is the angle between the reference line of the structure/body and the incoming fluid.

2.4.4 Critical Angle of Attack

The angle at which the maximum lift coefficient is obtained is called the critical angle of attack. Below this angle, the lift coefficient is directly proportional to the angle of attack.

2.4.5 Blockage Ratio

It is defined as the ratio of the area of the model/body which is perpendicular to the direction of flow to the cross-sectional area of the test section of the tunnel. It should be kept at less than 5% for better results.

2.4.6 Boundary Layer Thickness

It is defined as the separation from the wall of the rigid object calculated in y path to the position, where the rate of the flowing fluid is almost the same to 0.99X the free stream velocity.

2.5 Basic Formulae

2.5.1 Mass Flow Rate

It is the measure of the mass of the fluid passing through a point per unit time. Its unit is kg/s. Mathematically it is defined by the equation as,

$$M = \rho AV$$

2.5.2 Mass Ratio

It is defined as the ratio of the mass of the substance to the mass of fluid containing it. Mathematically it is written as,

$$MR = m1/m_o$$

2.5.3 Reynolds Number

Reynolds Number is the ratio of inertial forces to the viscous forces. Reynolds number give information whether the flow is laminar or turbulent. If the viscosity of the fluid is dominating over the inertia forces, then the flow is laminar. If the inertia force is dominating over the viscosity, then the flow is called turbulent flow. When the Reynolds Number is less than 2300, the flow is laminar and when Reynolds Number is greater than 4000, the flow is turbulent. Mathematically Re is defined by the formula;

$$Re = PVL/\mu$$

2.5.4 Cavitation Number

Cavitation number is defined as the difference between point pressure and vapor pressure of the fluid to its dynamic force. It is a dimensionless number.

2.5.5 Froude Number

It is a dimensionless number and is defined as the ratio of the inertial forces to the gravitational forces. Mathematically it is defined as;

$$Fr = \frac{U}{\sqrt{gd}}$$

2.5.6 Strouhal Number

It is defined as the ratio of the product of vortex shedding frequency and characteristic length to the velocity of the fluid. Mathematically it is written as

$$Sr = fL/U$$

2.5.7 Aspect Ratio

Aspect ratio is defined as the ratio of width to the height of an object. Mathematically it is written as,

$$AR = \frac{W}{H}$$

2.6 Forces Acting on the Flexible Structure in the Flowing Fluid

2.6.1 Drag Force

The force which is parallel but in the opposite direction to the relative motion of the body moving in a flowing fluid is called drag force. Drag force opposes the movement of the body through the fluid due to friction. Drag force varies directly with the square of the velocity of the moving body in the fluid. Mathematically it is defined by the formula give below,

$$F_D = \frac{1}{2}\,\rho C_D A V^2$$

Where ρ is the density of the fluid, C_D is the drag coefficient, A is the area of the body and V is the velocity of the fluid.

2.6.2 Lift Force

The force which acts at right angle to the direction of the fluid flow is called lift force. Lift force acts opposite to the weight force. Mathematically lift force is written as,

$$F_L = \frac{1}{2}\,\rho C_L A V^2$$

Where ρ is the density of the fluid, C_L is the lift coefficient, A is the area of the body and V is the velocity of the flow.

CHAPTER 3: EXPERIMENTAL SETUP

Overall schematics of the experimental setup are described in Figure 3.1(a). Experiments were performed in a low-speed water tunnel. The cross-section of the test section of the water tunnel was 600 × 400cm. The water tunnel was driven by a centrifugal pump. The velocity of the water in the tunnel varies from 0.1 to 0.5 m/s. The piezoelectric flag (description: DT2-028 K/L) with material properties as shown in Table 3.2 and details classification of material properties is shown in Table 3.1 was used as a flexible structure. The piezoelectric flags were attached to thin steel rods and the rods were clamped between two acrylic bars. The piezoelectric flags were placed in a conventional configuration, on a midline behind the bluff body in uniform flow with free trailing edge and clamped leading edge.

Table 3.1: Mechanical and Electrical Properties

Symbol	Parameter		PVDF	Units
T	Thickness		9, 28, 52, 110	µm (micron, 10-6)
d31			23	10-12
d33	Piezo Strain Constant		-33	
g31			216	10-3
g33	Piezo Stress constant		-330	
k31	Electromechanical Coupling		12%	
Kt	Factor		14%	
C	Capacitance		.com/.,mb380 for 28ìm	pF/cm2, @ 1KHz
Y	Young's Modulus		2-4	109 N/m2
V0	Speed of Sound	stretch:	1.5	
		thickness:	2.2	103 m/s
P	Pyroelectric Coefficient		30	10-6 C/m2 °K
Å	Permittivity		106-113	10-12 F/m
å/å 0	Relative Permittivity		12-13	

ρ_m	Mass Density	1.78	103kg/m
ρ_e	Volume Resistivity	>1013	Ohm meters
$R_\square$	Surface Metallization Resistivity	<3.0	Ohms/square for NiCu
$R_\square$		0.1	Ohms/square for Ag Ink
tan äe	Loss Tangent	0.02	@ 1KHz
	Yield Strength	45-55	106 N/m2 (stretch axis)
	Temperature Range	-40 to 80...100	$^\circ C$
	Water Absorption	<0.02	% H2O
	Maximum Operating Voltage	750 (30)	V/mil (V/µm), DC, @ 25°C
	Breakdown Voltage	2000 (80)	V/mil (V/µm), DC, @ 25°C

Table 3.2: Material Properties of the Piezoelectric Flag

Parameter	Units	Value
Capacitance @ 1KHz	pF/m	600
Acoustic Impedance	MRayl	4.0
Relative Permittivity	@1KHz	9
tan äe	@1KHz	0.017
Hydrostatic Piezo Coefficient	pC/N Vm/N	15
Longitudinal Piezo Coefficient	Vm/N	250×10^{-3}
Hydrostatic Piezo Coefficient		150×10^{-3}
Electromechanical Coupling	%	20

Energy Output	MJ/Strain (%)	10
Voltage Output	kV/Strain (%)	5

DAQ (a module in National Instrument Lab View) was used as a data acquisition system to calculate the voltage generated from the piezoelectric flags. Voltages were measured having a sampling rate = 50 with the number of samples to read = 50, which means that in one second it measures 50 samples of voltages. After acquiring data from the DAQ, the assistant pass the data to the indicator, it read the data in Lab View and displays it as a number or in the form of charts or bars for further processing.

An inverted C shaped circular cylinder of steel was used as a bluff body. The diameter of the cylinder was kept 25 mm to avoid blockage effect. The vortices having different vortex strength and different vortex shedding frequency strike on the surface of the piezoelectric flag, and the flag starts flapping. The distance between the bluff body and the piezoelectric flag is an important parameter to determine the flapping response of the piezoelectric flag. We varied the streamwise distance, G_x from 0.75 mm to 2.25 mm behind the inverted C shaped cylinder. The single flag gave maximum flapping amplitude and maximum voltage at Gx = 2. So the position of the upstream flag was fixed at this streamwise distance G_x (S/D) = 2 from the inverted C shaped cylinder. G_x was defined as the distance between the center of the cylinder and the leading edge of the piezoelectric flag to the diameter of the cylinder. The velocity of the flow was varied from 0.127 m/s to 0.257 m/s.

To acquire the images of the piezoelectric flags in flapping condition, the motion of the flags was recorded at 50 frames per second by using a high-speed camera, (Sony RX100 IV) mounted below the bottom of the test section. Two flashlights were used from both sides of the test section of water tunnel for the visualization of the flags in the flow, and the upper side of the test section was covered with black cloth to make the flag visible. Images were analyzed in MATLAB by using an image processing technique to determine the tail position of the flags in order to calculate the peak to peak amplitude (A/L) and superimposed images of the flags (flapping envelope) for the maximum and minimum flapping amplitude.

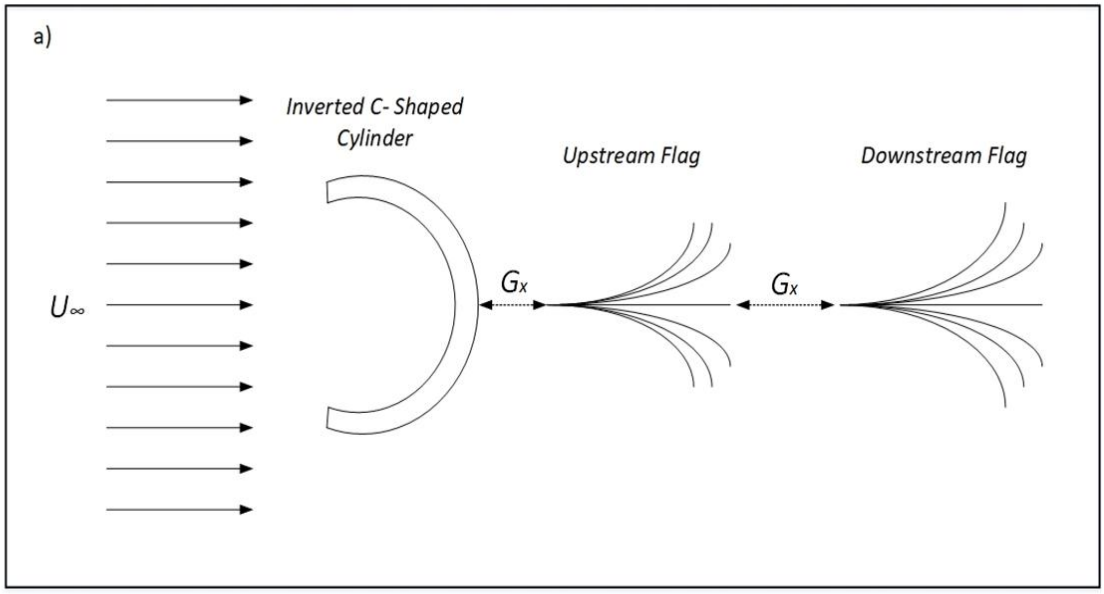

Figure 3.1(a): Schematic of two conventional piezoelectric flags in tandem configuration behind an inverted C-shaped cylinder.

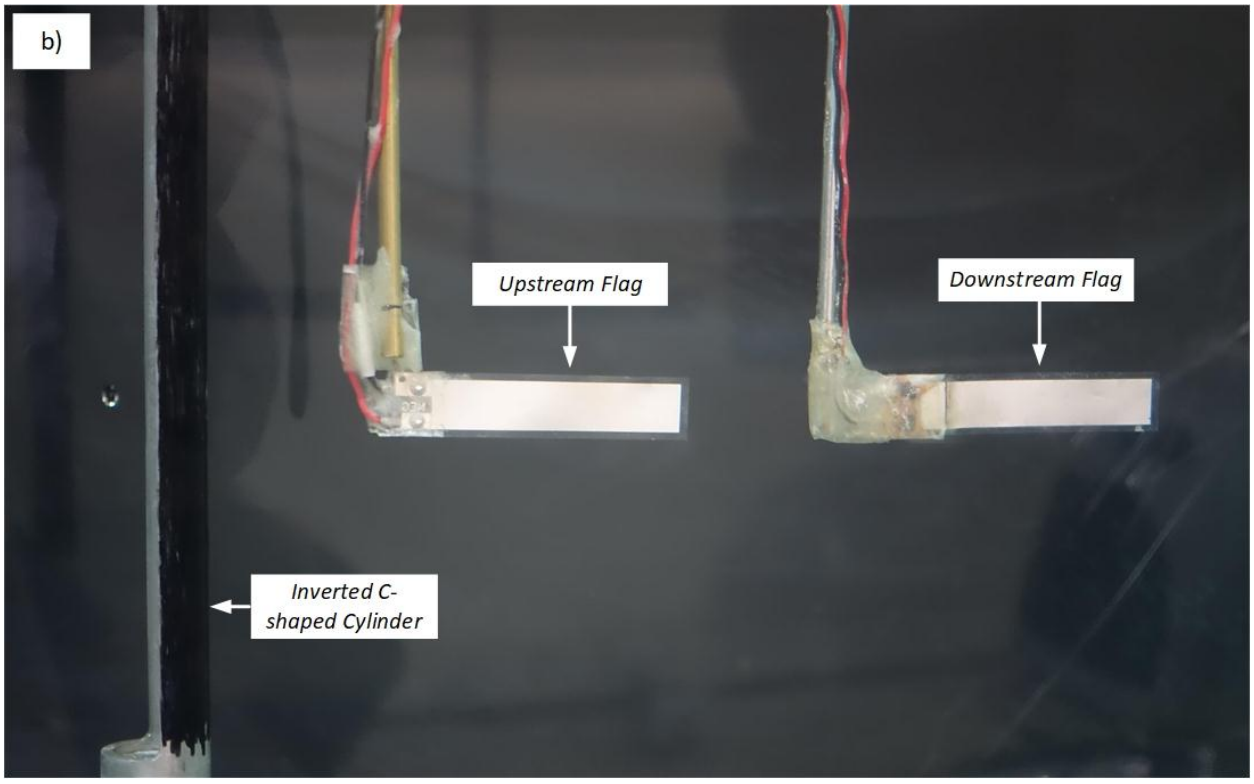

Figure 3.1(b): Two conventional piezoelectric flags in tandem configuration behind an inverted C-shaped cylinder in the test section of the water tunnel.

A list of the experiment was made first for the single piezoelectric flag and then for two tandem piezoelectric flags. i.e. for upstream flag and downstream flag.

T**able 3.3** shows the list of experiments for the six different velocities and six different streamwise gaps.

Table 3.3: List of Experiments

	Streamwise Distance (S/D)	**Velocity (m/s)**
Single Flag	0.75 1.25 1.50 1.75 2.0 2.25	0.127 0.153 0.178 0.205 0.230 0.257
Upstream Flag	2.0 2.0 2.0 2.0 2.0 2.0	0.127 0.153 0.178 0.205 0.230 0.257
Downstream Flag	0.75 1.25 1.50 1.75 2.0 2.25	0.127 0.153 0.178 0.205 0.230 0.257

CHAPTER 4: RESULTS AND DISCUSSIONS

We investigated the flapping dynamics and energy harvesting performance of two conventional piezoelectric flags in the tandem configuration behind an upstream inverted C shaped cylinder placed in a uniform fluid flow. In order to investigate the hydrodynamic interaction and behaviour of the two tandem conventional piezoelectric flags, the streamwise gap distance G_x (S/D ratio) between two flags was varied from 0.75 to 2.25. The flow velocity V was varied from 0.127 to 0.257 m/s. Below the velocity of 0.17 m/s, the flow was viscosity dominant and the flag does not show any significant flapping and remains in a straight mode. All the other variables were kept constant in this study. The position of the upstream flag behind the bluff body was kept constant at a distance $G_x = 2$, because at this streamwise distance the flag shows the maximum flapping amplitude and gives a maximum output voltage $V_{rms.}$

4.1 Effect of Velocity and Streamwise gap on Vrms, A/L and Flapping Frequency of Upstream Flag

The output voltage $V_{rms,}$ flapping frequency and flapping amplitude of the upstream piezoelectric flag as a function of the flow velocity and streamwise gap distance G_x are shown on a surface plot in figure 2. The point marked as M_x in figure 2(a) shows a maximum V_{rms} =1.06 Volts generated at a gap G_x =1.75 and velocity V =0.24 m/s. The corresponding points on figure 2(b) and figure 2(c) represents the maximum flapping frequency of 0.067 rad/sample and corresponding maximum flapping amplitude (A/L) of 1.04. The higher flapping frequency and peak to peak amplitude (A/L) produces a large deformation in the piezoelectric flag which leads to higher voltage generation in a piezoelectric flag [7]. Below G_x =1.75, the flag showed a decrease in the voltage produced at low velocities. The reason for low voltage was the lower flapping frequency and flapping amplitude, which produces a smaller deformation in the piezoelectric flag at low velocities. Similarly, in figure 2(a) the point marked as M_n represents a minimum voltage V_{rms} =0.19 Volts at a distance, G_x =1.25 & velocity V=0.13 m/s. It is clear from figure 3(d), where the flag envelope has a low flapping amplitude. Figure 2(b) and figure

2(c) also show the minimum flapping frequency of 0.003 and minimum flapping amplitude A/L of 0.31 respectively. The strain energy induced in the piezoelectric flag is proportional to the velocity of the fluid and flapping amplitude of the flag and the maximum bending deformation produced in the flag. As we increase the velocity of the flow, the strain energy induced in the piezoelectric flag also increases and as a result the output voltage increases. The smaller flapping amplitude of the flag induces the smaller deformation and strain energy and larger flapping amplitude of the flag induces greater strain energy and bending deformation in the flag.

In the conventional piezoelectric flag as flow velocity increases, the flapping amplitude of the flag increases until the flapping behaviour of the flag goes from periodic flapping mode to the non-periodic flapping mode, while in the case of the inverted flag as flow velocity increases, the flapping behaviour of flag changes from periodic flapping mode to the deflected mode [3]. It was observed that when $G_x < 1.25$, the drag force of the front flag is also reduced due to the close presence of the rear flag.

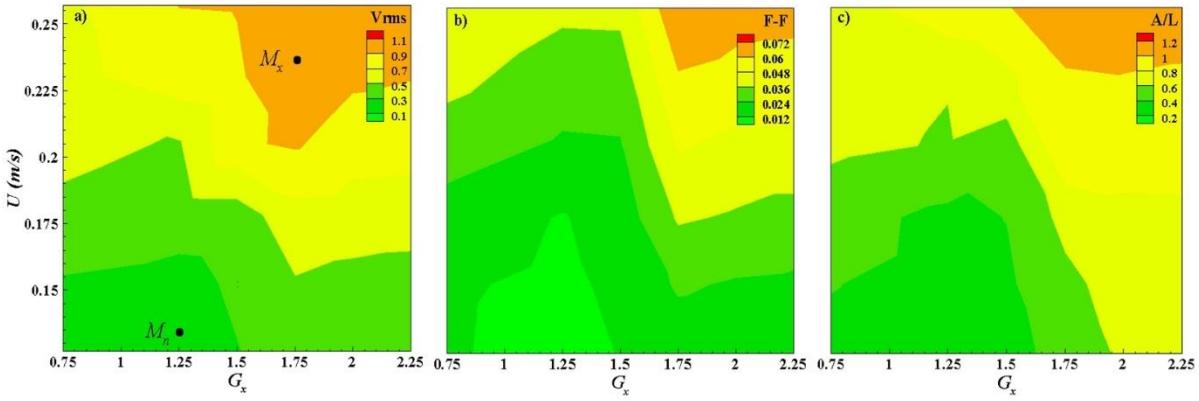

Figure 4.1: (a) Surface plot of root mean square voltage Vrms ranging from 0.1 to 1.1 Volts. (b) Maximum Flapping frequency ranging from 0.012 to 0.072. (c) Maximum Peak-to-peak amplitude (A/L) ranging from 0.2 to 1.2.

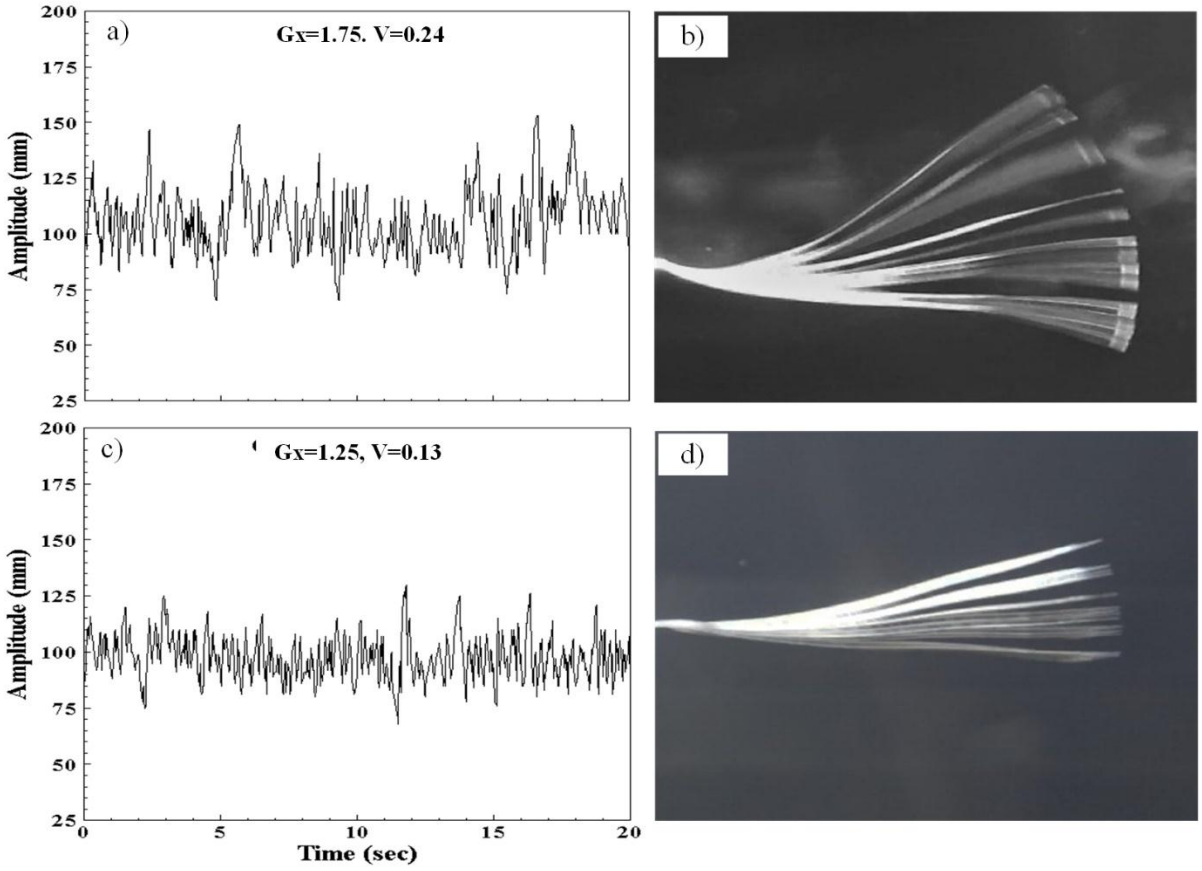

Figure 4.2: (a) Time history of the maximum flapping amplitude (b) Superimposed images of flag at G_x = 1.75 and V = 0.24 m/s (c) Time history of minimum flapping amplitude (d) Superimposed images of flag at G_x = 1.25 and V = 0.13 m/s.

We also calculated the energy density of the signal for the maximum and minimum dominant flapping frequency by using Fast Fourier Transform (FFT), as shown in figure 4.3 and figure 4.4.

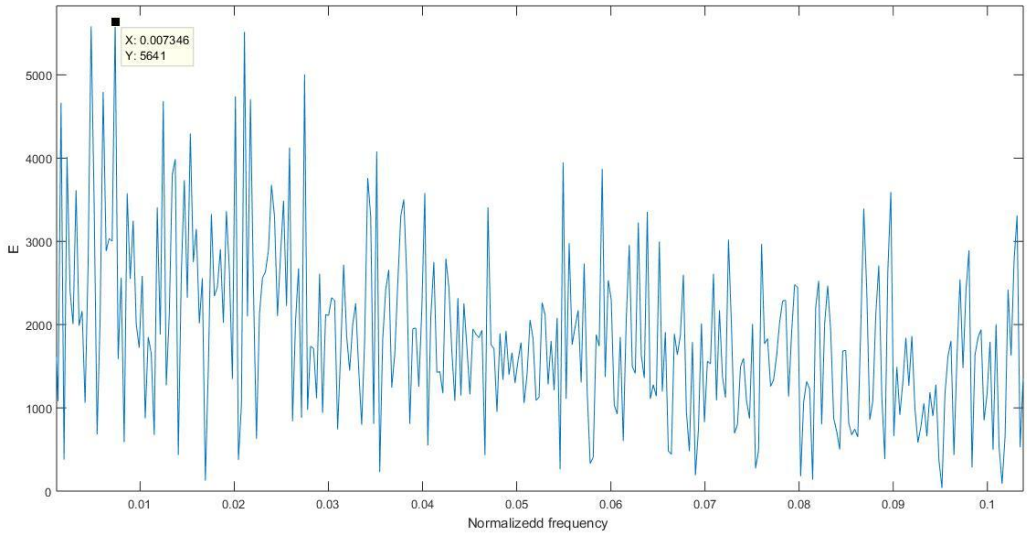

Figure 4.3: Energy spectrum of the maximum flapping dominant frequency.

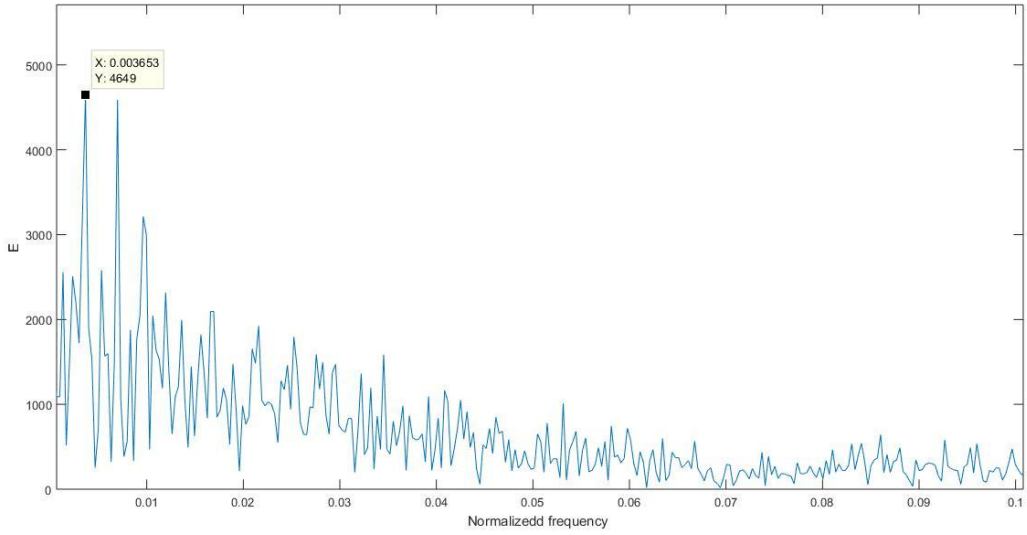

Figure 4.4: Energy spectrum of the minimum flapping dominant frequency.

4.2 Effect of Velocity and Streamwise gap on Vrms, A/L and Flapping Frequency of Downstream Flag

The output voltage $V_{rms,}$ flapping frequency and flapping amplitude of the downstream piezoelectric flag as a function of the streamwise gap distance G_x and flow velocity are shown on a surface plot in figure 4.5. The point labeled as M_x in figure 4.5(a) represents a maximum voltage, V_{rms} =1.16 Volts generated at streamwise gap G_x = 1.75, and the corresponding points on figure 4.5(b) and figure 4.5(c) represents maximum flapping frequency of 0.070 rad/sample and corresponding maximum flapping amplitude (A/L) of 1.12. When the flow velocity was increased from 0.153 m/s, the vortex shedding from the inverted C shaped cylinder become stronger. By increasing the flow velocity, the vortex decreases in the size but the number of vortices shedding from the upstream flag increases.

The flapping amplitude of the downstream flag was found to be larger than the upstream flag at the same flow velocity because the wake behind the upstream flag interact with the downstream flag and drove synchronization in the flapping of the downstream flag [13]. The large flapping amplitude caused the downstream flag to experience more drag force than the upstream flag. So the flapping of downstream flag was more energetic and had a larger flapping amplitude. For tandem flags, inverted drafting was observed which leads to the small flapping amplitude for the upstream flexible flag and significantly a larger flapping amplitude for the downstream flag. Inverted drafting phenomena occur in flexible structures placed in a fluid flow in which the drag force on one flag is increased by excitation from the wake of another flag. Inverted drafting occurs when the wakes of the flags add coherently to form stronger vortices. For the range of streamwise gap, $0.75<G_x<1.75$, the flapping amplitude (A/L) the of downstream flag decreases for lower velocities and for the streamwise gap G_x >1.75, the flapping amplitude increases significantly. The voltage generated was increased for the streamwise gap in the range G_x = 1.25 to 2.25. In figure 4.5(a) the point labeled as M_n represents a minimum V_{rms} = 0.23 Volts at the gap G_x = 1.25 & flow velocity V = 0.15 m/s and the corresponding region on figure 4.5(b) and figure 4.5(c) show the minimum flapping frequency of 0.0036 and minimum flapping amplitude A/L of 0.34 of the downstream flexible flag respectively.

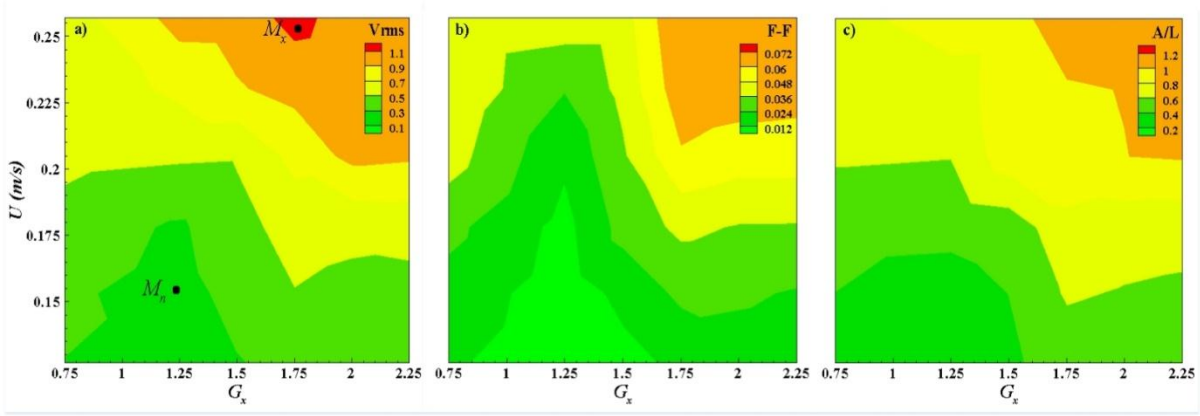

Figure 4.5: (a) Surface plot of root mean square voltage Vrms ranging from 0.1 to 1.1 Volts. (b) Maximum Flapping frequency ranging from 0.012 to 0.072. (c) Maximum Peak-to-peak amplitude (A/L) ranging from 0.2 to 1.2.

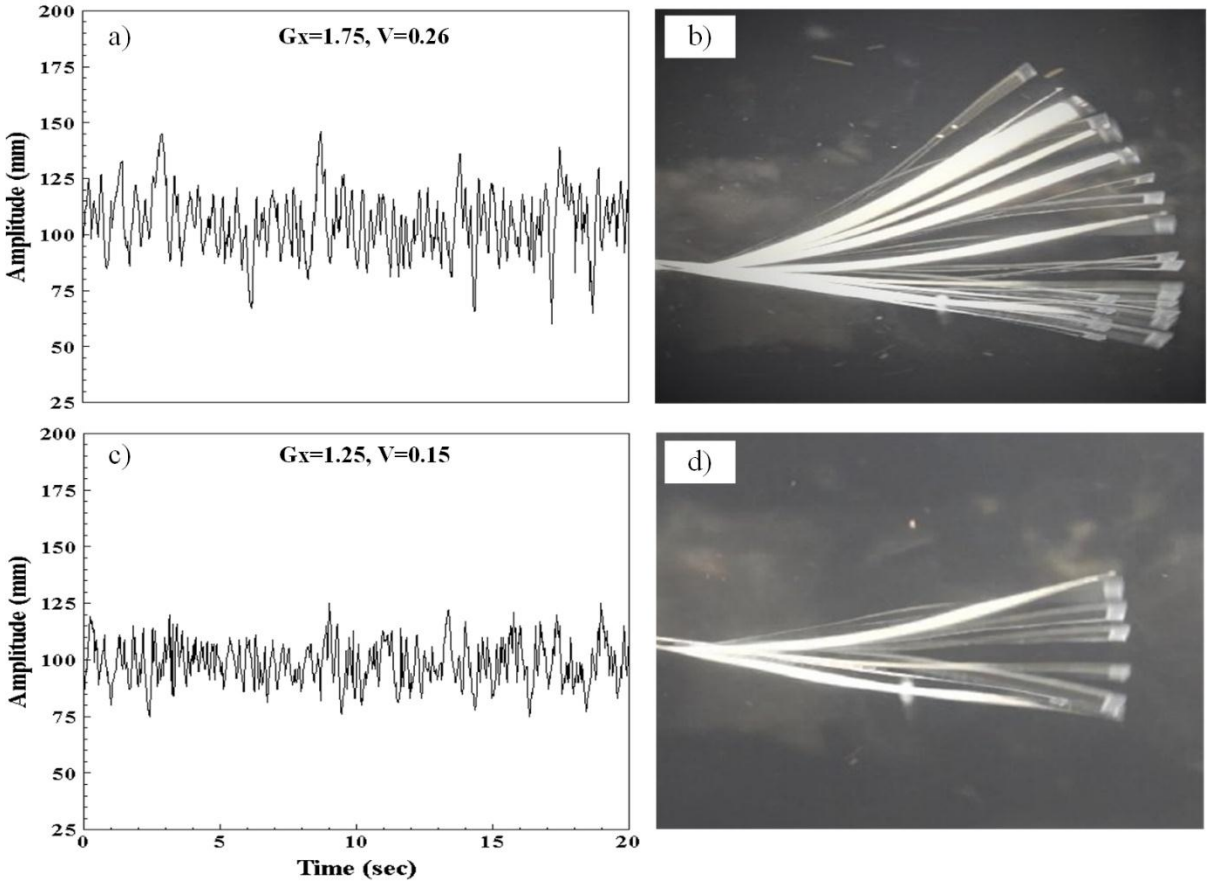

Figure 4.6: (a) Time history of the maximum flapping amplitude (b) Superimposed images of flag at Gx = 1.75 and V = 0.26 m/s. (c) Time history of minimum flapping amplitude (d) Superimposed images of flag at Gx = 1.25 and V = 0.15 m/s.

We also calculated the energy density of a signal for the maximum and minimum dominant flapping frequency by using Fast Fourier Transform (FFT) in the MATLAB, as shown in figure 4.7 and figure 4.8.

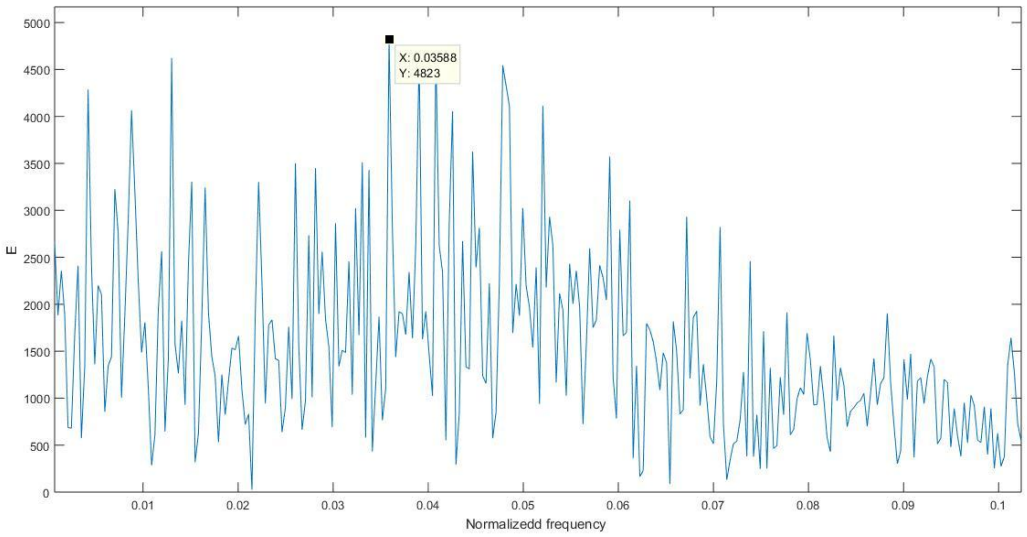

Figure 4.7: Energy spectrum of the maximum flapping dominant frequency.

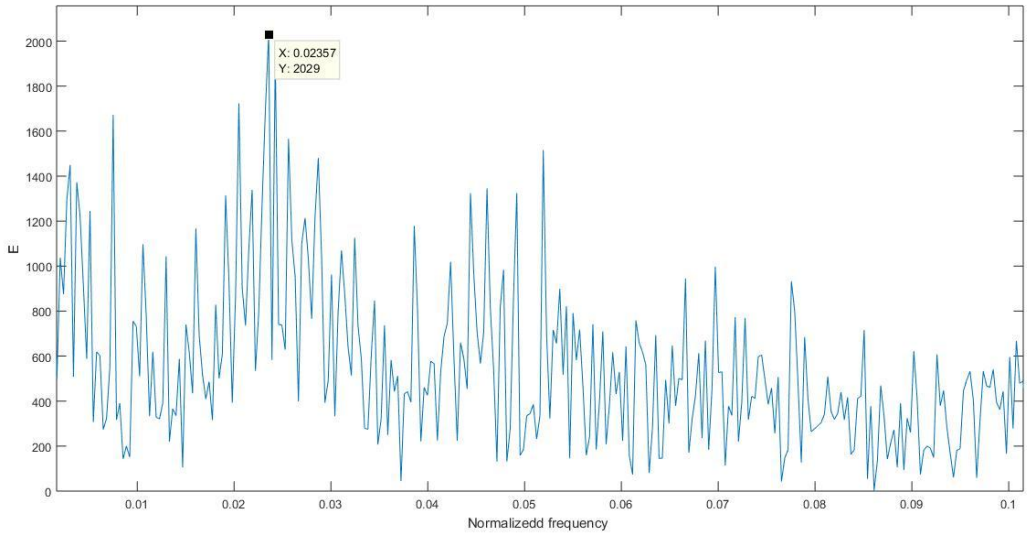

Figure 4.8: Energy spectrum of the minimum flapping dominant frequency.

4.3 Comparison of the Upstream And Downstream Flags

The bending deformation produced in the piezoelectric flag depends on many factors such as flow velocity, bending stiffness, bending coefficient, vortex shedding frequency, vortex strength, length, width and thickness of piezoelectric flag and fluid pressure, so we experience different output voltage V_{rms} for different flow velocity and streamwise gaps. If we compare the flapping amplitude and the voltage produced by both flags, then the downstream flag shows a larger flapping amplitude and output voltage as compared to the upstream flag. The difference between the flapping amplitude of the upstream and downstream flags is explained by the vortex structures and vortex merging mode in the wake of both flags behind the cylinder. Vortices shedding from the upstream flag and downstream flag interact and merge with each other either in constructive or destructive manner.

It was observed that the downstream flag showed a different range of deformations at different flow velocities with the same bending coefficients for both flags. The different range of bending deformations produced in the downstream flag at a constant bending coefficient arise from variations in the flow velocity and the presence of the upstream flag in front of downstream flag. Variations in the relative bending deformations in the upstream and downstream flexible

flags can be explained from two interaction modes of vortices shedding from the upstream and downstream flexible flags. The interaction between the vortices shedding from two flexible flags and flow effects the forces experienced by the piezoelectric flags by one of the two modes: (i) a constructive mode and (ii) a destructive mode. These modes vortex interaction were first explained by Gopalkrishnanet during the study of active vorticity control using a flapping foil behind a circular cylinder in a flow [4]. In this study, the authors find out three modes of vortex interaction and noted that the vortices generated from the bluff body were repositioned by the suction generated by the foil. The constructive vortex merging mode explains the situation in which vortices that are shed by the downstream flexible flag combine with vortices having the same rotational sense produced by the upstream flag. The blending of the vortices of the same rotation produces vortices having greater strength. In contrast to the constructive mode, the destructive mode describes the blending of vortices that are rotating in opposite direction, produced by the upstream and downstream flexible flags. This results in a weaker merged vortex having decreased strength.

In the constructive merging mode of vortices, the downstream flag encountered incoming vortices produced from the upstream flag. The downstream flag was moved not only by the vortices produced by the downstream flag, but also by the incoming vortices, which merged in a constructive manner, due to which the flapping amplitude of flag increases. In the destructive merging mode, the vortices rotating in anti-clockwise direction which are generated from the downstream flag merge with the incoming vortices rotating in the clockwise direction produced from the upstream flag. The vortices formed after destructive merging mode results in the weaker vortices, which decreases the flapping amplitude of the downstream flag. We can say that tandem flags in the conventional configuration experienced alternating constructive and destructive vortex merging modes.

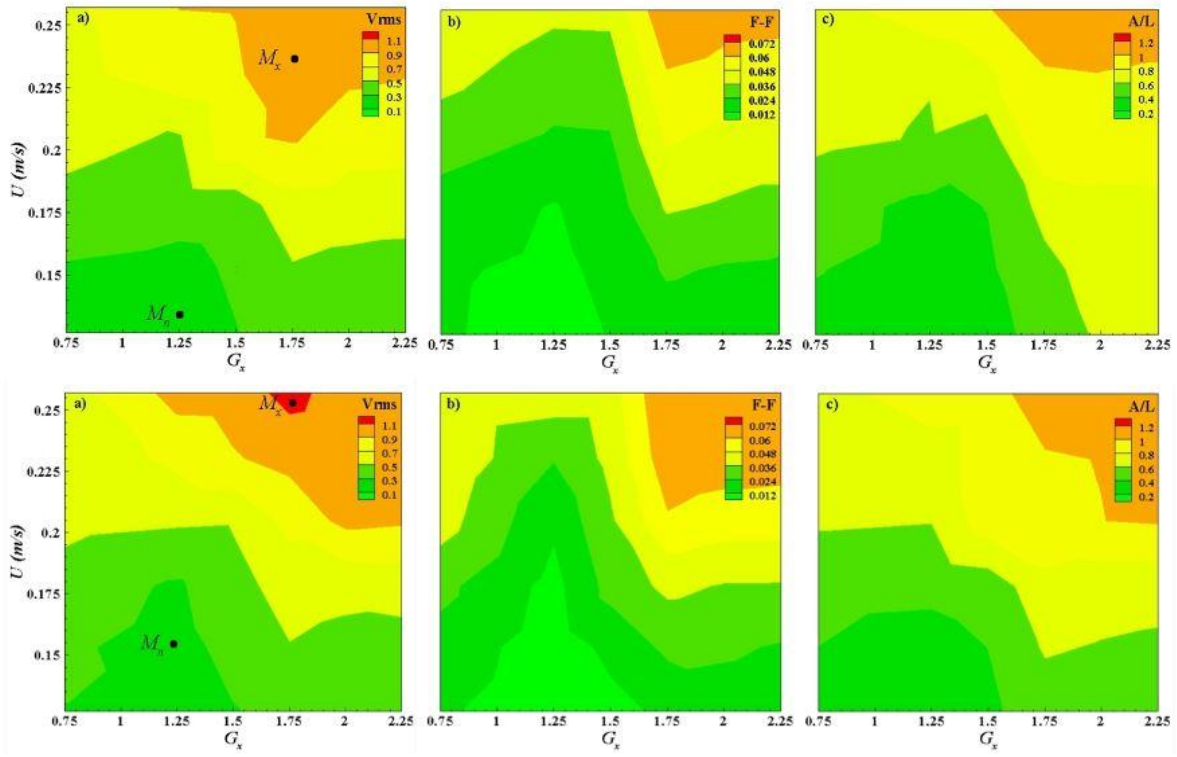

Figure 4.9: Surface Plot of both flags, Vrms, Flapping frequency and Peak to peak amplitude.

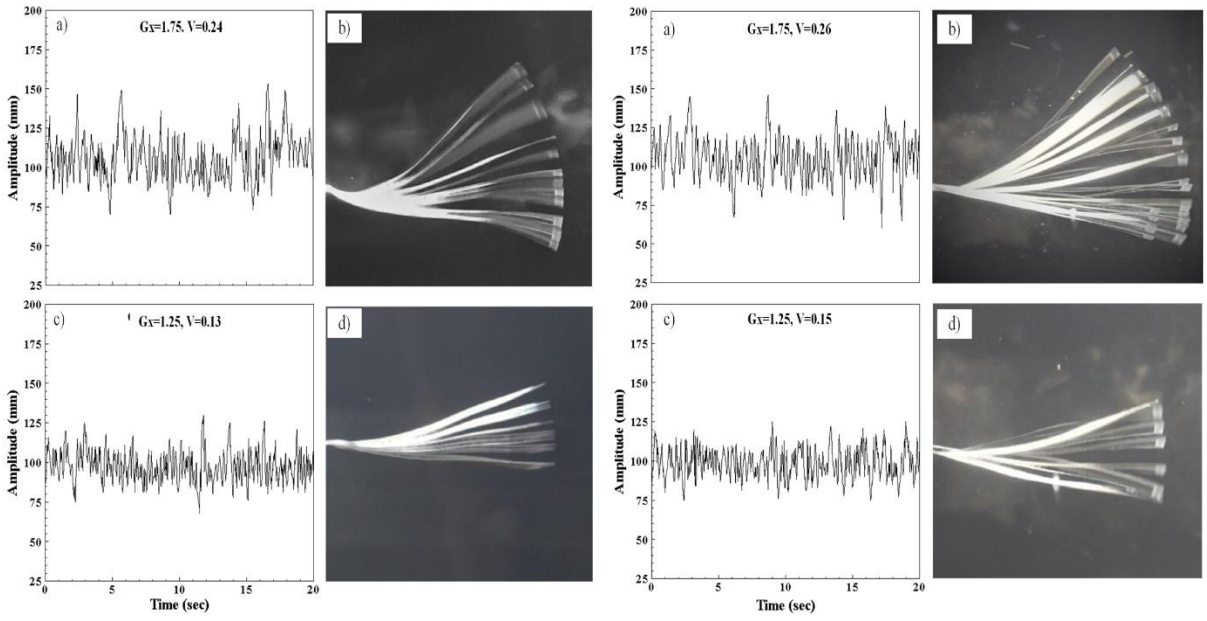

Figure 4.10: Time history of the maximum and minimum flapping amplitude and superimposed images of the upstream and downstream flags.

4.4 PIV Results

Particle image velocimetry is widely used for the visualization of the flow and also for the measurement of the flow velocity. The flow is treated with the tracer particles of very small size for the visualization of the flow. The tracer particles illuminate the flow field. PIV technique was used to see the vortices produced, their behavior and their interaction with the piezoelectric flags behind the bluff body. We used an inverted C shaped cylinder as a bluff body for the generation of vortices and to study their effect on the piezoelectric flags and to investigate the constructive interaction merging mode and destructive vortex merging mode between vortices produced from the upstream and downstream flags.

We performed the particle image velocimetry for the cases in which we got maximum output voltage. The results of the PIV are shown below.

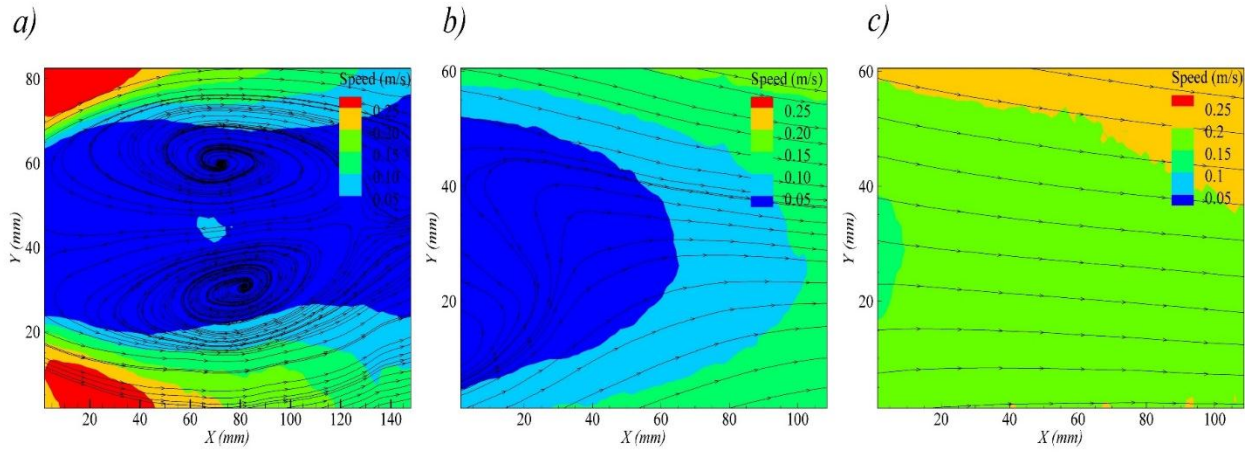

Figure 4.11: (a) Velocity field behind the cylinder. (b) Velocity field behind the upstream flag. (c) Velocity field behind the downstream flag.

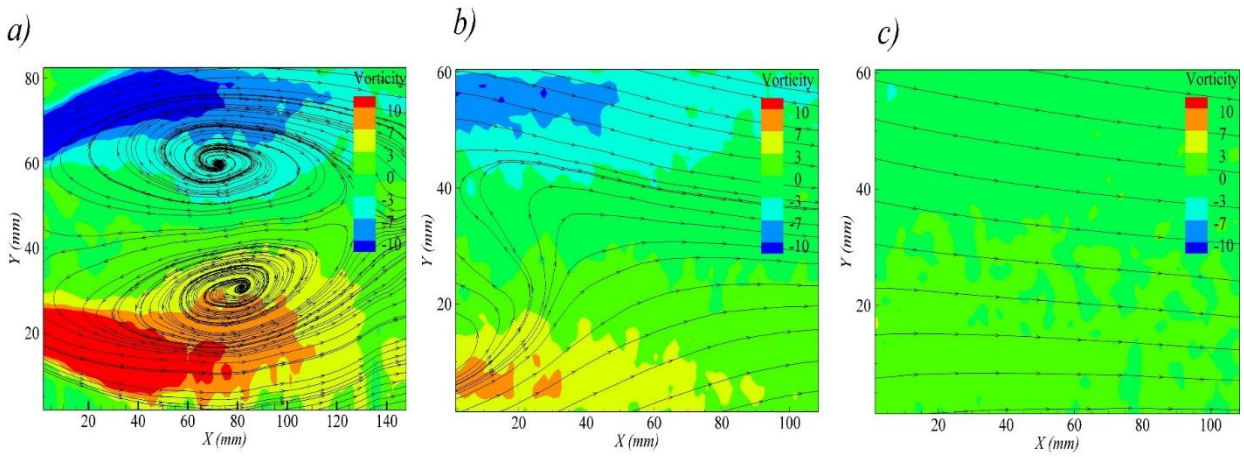

Figure 4.12: (a) Vorticity contours behind the cylinder. (b) Vorticity contours behind the upstream flag. (c) Vorticity contours behind the downstream flag.

The value of the velocity field of the downstream flag is higher as compared to the velocity field of the upstream flag. So the output voltage and flapping amplitude of the downstream flag is higher than the upstream flag. The value of vorticity was greater behind the cylinder as compared to the vorticity values behind the flags. The surface plot of velocity shows that the alternating vortices were formed behind an inverted C shaped cylinder and they impart their energy to the piezoelectric flag when they strike with the surface of the piezoelectric flag. The vortices coming from the right side of the cylinder try to move the flag in the downward direction and the vortices coming from the left side of the cylinder tend to move the flag in an upward direction. These vortices are shed periodically and when they strike with the surface of the piezoelectric flag, the flag starts to flap in a periodic manner.

CHAPTER 5: CONCLUSION

The energy harvesting performance of two tandem conventional piezoelectric flags in uniform flow was experimentally investigated in this study. The conventional flags have clamped leading edges and free trailing edges. Experiments were performed by varying the streamwise gap distance G_x (S/D) between the flags from 0.75 to 2.25 mm. Maximum voltage (Vrms= 1.18 volts) was achieved in case of a single flag at S/D= 2 and V= 0.23 m/s where maximum vortex shedding occurs as confirmed by PIV results. The value of vorticity is higher near the cylinder as shown in PIV results. Similarly, minimum voltage (Vrms= 0.11 volts) was also achieved in case of single flag at S/D= 1.5 and V= 0.153 m/s. It was observed that the maximum voltage for both upstream and downstream flags was achieved in the gap between 1.25 to 2.0 and velocity above 0.2 m/s.

Maximum and minimum voltage region for the upstream flag and downstream flag was similar following the similar flapping amplitude region and flapping frequency region. For smaller $G_{x,}$ the flapping amplitude of the rear flag was reduced due to destructive vortex merging mode between vortices.

The downstream flag showed larger flapping amplitude, flapping frequency and output voltage V_{rms} for $G_x \geq 1.5$. This was caused by the constructive interaction merging mode between vortices.

The flapping amplitude and V_{rms} of both the flags increased from G_x = 1.5 to 2.25. It was found that for smaller G_x the flapping amplitude of rear flag was reduced due to the interaction of the tandem flags which is due to the destructive vortex merging mode. It was also identified that the downstream flag showed the larger flapping amplitude and output voltage V_{rms} for $G_x \geq 1.5$ as compared to the upstream flag. This was caused by the constructive interaction merging mode between vortices at these separation distances, which increases the flapping amplitude and flapping frequency, and consequently the output voltage of the flag.

REFERENCES

[1] Akaydın, H., Elvin, N., & Andreopoulos, Y. (2010). Wake of a cylinder: a paradigm for energy harvesting with piezoelectric materials. *Experiments in Fluids, 49*(1), 291-304.

[2] Allen, J., & Smits, A. (2001). Energy harvesting eel. *Journal of fluids and structures, 15*(3-4), 629-640.

[3] Cossé, J., Sader, J., Kim, D., Cerdeira, C. H., & Gharib, M. (2014). *The effect of aspect ratio and angle of attack on the transition regions of the inverted flag instability.* Paper presented at the ASME 2014 Pressure Vessels and Piping Conference.

[4] Gopalkrishnan, R., Triantafyllou, M. S., Triantafyllou, G. S., & Barrett, D. (1994). Active vorticity control in a shear flow using a flapping foil. *Journal of Fluid Mechanics, 274*, 1-21.

[5] Kim, D., Cossé, J., Cerdeira, C. H., & Gharib, M. (2013). Flapping dynamics of an inverted flag. *Journal of Fluid Mechanics, 736*.

[6] Kollmann, W., & Umont, G. (2004). *Lamb vector properties of swirling jets.* Paper presented at the Fifteenth Australasian fluid mechanics conference, Sydney, Australia.

[7] Lamb, & Horace, S. (1945). *Hydrodynamics* (Sixth edition ed.): N.Y., Dover Publications.

[8] Michelin, S., & Doaré, O. (2013). Energy harvesting efficiency of piezoelectric flags in axial flows. *Journal of Fluid Mechanics, 714*, 489-504.

[9] Orrego, S., Shoele, K., Ruas, A., Doran, K., Caggiano, B., Mittal, R., & Kang, S. H. (2017). Harvesting ambient wind energy with an inverted piezoelectric flag. *Applied energy, 194*, 212-222.

[10] Ristroph, L., & Zhang, J. (2008). Anomalous hydrodynamic drafting of interacting flapping flags. *Physical review letters, 101*(19), 194502.

[11] Shahbazi, Y., Chenaghlou, M. R., Abedi, K., Khosrowjerdi, M. J., & Preumont, A. (2012). A new energy harvester using a cross-ply cylindrical membrane shell integrated with PVDF layers. *Microsystem Technologies, 18*(12), 1981-1989.

[12] Uddin, E., Huang, W.-X., & Sung, H. J. (2015). Actively flapping tandem flexible flags in a viscous flow. *Journal of Fluid Mechanics, 780*, 120-142.

[13] S. Alben and M. J. Shelley, "Flapping states of a flag in an inviscid fluid: Bistability and the transition to chaos," *Fluid Dyn. Res.*, vol. 46, no. 5, pp. 3–6, 2014.

[14] M. Nishioka and H. Sato, "Mechanism of determination of the shedding frequency of vortices behind a cylinder at low Reynolds numbers," *J. Fluid Mech.*, vol. 89, no. 1, pp. 49–60, 1978.

[15] A. Maas, "Local and global gauge-fixing," *Proc. Sci.*, pp. 473–537, 2012.

[16] M. Gaster, "Vortex shedding from circular cylinders at low Reynolds numbers," *J. Fluid Mech.*, vol. 46, no. 4, pp. 749–756, 1971.

[17] J. H. Lienhard, "Synopsis of lift, drag, and vortex frequency data for rigid circular cylinders," *Bulletin 300*. pp. 1–36, 1966.

[18] C. K. Choi and D. K. Kwon, "Wind tunnel blockage effects on aerodynamic behavior of bluff body," *Wind Struct. An Int. J.*, vol. 1, no. 4, pp. 351–364, 1998.

[19] E. Uddin, W. X. Huang, and H. J. Sung, "Interaction modes of multiple flexible flags in a uniform flow," *J. Fluid Mech.*, vol. 729, pp. 563–583, 2013.

[20] C. B. Sun, S. Y. Wang, L. B. Jia, and X. Z. Yin, "Force measurement on coupled flapping flags in uniform flow," *J. Fluids Struct.*, vol. 61, pp. 339–346, 2016.

[21] B. S. H. Connell and D. K. P. Yue, *Flapping dynamics of a flag in a uniform stream*, vol. 581. 2007.